Journal of Geochemical Exploration 197 (2019) 70–83

Contents lists available at ScienceDirect

Journal of Geochemical Exploration

journal homepage: www.elsevier.com/locate/gexplo

Sulfur and lead isotopic variations in the giant Yulong porphyry Cu (Mo−Au) deposit from the eastern Tibetan Plateau: Implications for origins of S and Pb, and metal precipitation

Ming-Liang Huang[a,b], Xian-Wu Bi[a,*], Jian-Feng Gao[a], Lei-Luo Xu[a], Jia-Fei Xiao[a], Shen-Tai Liu[c], Xin-Song Wang[a], Ting Zhou[a]

[a] State Key Laboratory of Ore Deposit Geochemistry, Institute of Geochemistry, Chinese Academy of Sciences, Guiyang 550081, China
[b] University of Chinese Academy of Sciences, Beijing 100049, China
[c] Tibet Yulong copper industry Company Ltd, Tibet, Changdu 854100, China

ARTICLE INFO

Keywords:
Yulong porphyry Cu (Mo−Au) deposit
S and Pb isotopes
Ore-forming materials

ABSTRACT

The giant Yulong porphyry Cu (Mo−Au) deposit, located in the eastern Tibetan Plateau, is a typical post-subduction porphyry Cu ± Mo ± Au deposit formed in an intracontinental strike-slip fault system, and it is also one of the largest porphyry Cu deposits in China with reserves of 6.5Mt Cu @ 0.62% and 0.41Mt Mo @ 0.042%, respectively. In this study, sulfur and lead isotopic compositions of sulfides and ore-related porphyry samples were determined to constrain the sources of ore-forming materials and ore-forming process. Sulfides (e.g., pyrite, chalcopyrite and molybdenite) from phyllic alteration zone, where the Cu and Mo mineralization mainly occurred, have uniform $\delta^{34}S$ values ranging from −0.6 to +2.1‰ (average + 1.1‰), which indicates a magmatic origin of the sulfur. In situ Nano-SIMS sulfur isotope analysis further reveals that pyrites formed in potassic alteration stage have systematically negative $\delta^{34}S$ values ranging from −0.2 to −9.7‰ (average − 4.5‰), whereas pyrites formed in phyllic alteration stage have systematically positive $\delta^{34}S$ values ranging from +1.1 to +3.2‰ (average + 2.1‰). This regular variation is considered to be resulted from disproportionation of aqueous SO_2 and subsequent sulfate reduction, further suggesting a magmatic origin of the sulfur. The sulfides have initial Pb isotopic compositions ($(^{206}Pb/^{204}Pb)_i$ = 18.616–18.812, $(^{207}Pb/^{204}Pb)_i$ = 15.670–15.740, $(^{208}Pb/^{204}Pb)_i$ = 38.956–39.080) deviating from those of the ore-related porphyries ($(^{206}Pb/^{204}Pb)_i$ = 18.549–18.718, $(^{207}Pb/^{204}Pb)_i$ = 15.647–15.662, $(^{208}Pb/^{204}Pb)_i$ = 38.794–39.888), but more close to those of the ore-hosting strata ($(^{206}Pb/^{204}Pb)_i$ = 18.423–18.761, $(^{207}Pb/^{204}Pb)_i$ = 15.654–15.713, $(^{208}Pb/^{204}Pb)_i$ = 38.867–39.062). The shift of Pb isotopic compositions of sulfide minerals toward those of ore-hosting strata indicates that the ore-hosting strata had provided a significant amount of Pb for ore formation, and most probably suggests fluid-rock interaction processes in the hydrothermal system. Our study represents a case study in which ore-hosting strata had provided a significant amount of ore-forming materials for porphyry Cu ± Mo ± Au formation in the post-subduction setting.

1. Introduction

Porphyry Cu ± Mo ± Au deposits are defined as large volumes of hydrothermally altered rocks centered on porphyry Cu stocks with depth of 2–5 km in the upper crust (Sillitoe, 2010). They are typically formed in both oceanic slab subduction-related arc-settings and post-subduction settings (Bi et al., 2002, 2004, 2005, 2009; Cooke et al., 2005; Hou et al., 2009, 2011, 2013; Richards, 2003, 2009, 2011; Shafiei et al., 2009; Sillitoe, 2010; Xu et al., 2011, 2012, 2016), and derive their ore-forming materials (e.g., fluids, S, Cl, and metals) predominantly from ore-related porphyry magmas (Hou et al., 2013; Pettke et al., 2010; Richards, 2003, 2011; Sillitoe, 1972, 2010; Xu et al., 2016).

Nevertheless, there are clear evidences from sulfur and lead isotopes showing that wall-rocks may have also provided partial ore-forming materials for porphyry Cu ± Mo ± Au deposits in oceanic slab subduction-related arc-settings (Bouse et al., 1999; Chiaradia, 2004; Cooke et al., 2014; Dilles et al., 1995; Force, 1998; Mukasa et al., 1990; Richards et al., 1991), and the examples include the giant Butte porphyry Cu−Mo deposit in USA (Field et al., 2005), the Porgera porphyry

* Corresponding author.
E-mail address: bixianwu@mail.gyig.ac.cn (X.-W. Bi).

https://doi.org/10.1016/j.gexplo.2018.11.019
Received 14 January 2018; Received in revised form 6 September 2018; Accepted 26 November 2018
Available online 29 November 2018

Au deposit in Papua New Guinea (Richards et al., 1991), and the Miocene porphyry Cu deposits in Ecuador (Chiaradia, 2004). Based on systematical lead isotope comparison between wall-rocks, ores and porphyries, Cooke et al. (2014) argued that it is common for porphyry Cu formation that wall-rocks have contributed the ore-forming materials to porphyry Cu systems to varying degrees, and that this effect is clearer where wall rocks have a Pb isotopic contrast to the porphyry magmas. The abovementioned phenomenon reflects local fluid-rock interaction between the magmatic fluids and the isotopically different wall-rocks during hydrothermal circulation in the shallow crust (Cooke et al., 2014; Mukasa et al., 1990; Richards et al., 1991; Tosdal et al., 1999). Therefore, sulfur and lead isotope studies allow us to better understand the ore-related magmatic-hydrothermal processes for porphyry Cu ± Mo ± Au deposits.

The giant Yulong porphyry Cu (Mo−Au) deposit, located in the eastern Tethyan metallogenic domain (Richards, 2015), is a typical post-subduction porphyry Cu deposit that was formed in an intracontinental strike-slip fault system at Eocene (Hou et al., 2003; Xu et al., 2012, 2016); it is one of the largest porphyry Cu deposits in China with a reserve of 6.5 Mt. Cu @0.62% and 0.41 Mt. Mo @ 0.042% (Tibet Yulong Copper Co. Ltd., 2009). Zircon U−Pb dating (41.0–43.8 Ma; Chang et al., 2017; Guo et al., 2006; J.X. Li etal., 2012; Liang et al., 2006; Xu et al., 2012) and molybdenite Re−Os dating (37.15–42.28 Ma; Chang et al., 2017; Hou et al., 2006; Tang et al., 2009) of the Yulong deposit indicate a close genetic relationship between the Cu (Mo−Au) mineralization and the ore-bearing monzogranite porphyry. Published H-O-S (Gu et al., 2003; Hou et al., 2007) and He−Ar (Hu et al., 2004) isotopes further suggest that the ore-forming fluids and materials are sourced from the mantle-derived monzogranite porphyry. Nonetheless, whether the wall-rocks have contributed the ore-forming materials or not remains unclear due to the lack of relevant data, especially the Pb isotopes of the sulfides and wall rocks.

In the present study, based on the Pb isotopes of sulfides, ore-related porphyries and ore-hosting strata, we report the evidence that ore-hosting strata had provided a certain amount of ore-forming materials for the formation of the giant Yulong porphyry Cu (Mo−Au) deposit. This represents a case study demonstrating that ore-hosting strata have contributed some of the ore-forming materials to porphyry Cu ± Mo ± Au deposits in the post-subduction setting. Furthermore, through systematic sulfur isotope analysis of sulfides and different generations of pyrites, a regular variation in the sulfur isotopes from the early ore-stage to the late ore-stage is observed for the Yulong deposit. We suggest that such a variation is resulted from disproportionation of magma SO_2 and magma sulfate reduction, which indicates the magmatic origin of the sulfur.

2. Geological background

2.1. Regional geology

The Tibetan plateau was formed by aggregation of the Songpan-Ganzi, Qiangtang, and the Lhasa terranes from north to south (Fig. 1; Yin and Harrison, 2000). The Qiangtang terrane is bordered by the Songpan-Ganzi in the north and Lhasa terrane in the south, and these terranes are separated by the Triassic Jingshajiang-Red river suture to the north (Zhu et al., 2011; Zi et al., 2012a, 2012b), and Bangonghu-Nujiang suture to the south (Kapp et al., 2005; Yin and Harrison, 2000; Fig. 1). The eastern Qiangtang terrane, where the Yulong porphyry Cu−Mo deposit is located, is composed of the Changdu-Simao block, and Jiangda-Weixi arc in the east and the Zuogong-Jinghong arc in the west (Fig. 2a). Formation of the Jiangda-Weixi arc and the Zuogong-Jinghong arc are related to subduction of the Jinshajiang and Lancanjiang Pale-Tethyan oceanic slab, respectively (Tang and Luo, 1995). The Changdu-Simao block consists of the Proterozoic crystalline basement and an Early Paleozoic folded basement and cover rocks a continuous, but badly damaged platform transitional facies (carbonate and clastic sedimentary rocks) from the Devonian to Cretaceous (Tang and Luo, 1995).

The Cenozoic Indo-Asian collision gave rise to a series of large-scale strike-slip faults and overthrust systems in the eastern Tibetan Plateau and its surrounding areas (Hou et al., 2003; Liang et al., 2006; Xu et al., 2012); During this period, numerous alkaline igneous rocks were emplaced or erupted along and within these strike-slip fault systems, forming the over 2000 km long and 50–80 km wide Jinshajiang-Red river alkaline igneous belt and associated porphyry Cu ± Mo ± Au deposits (e.g., Yulong, Malasongduo, Duoxiasongduo, Machangqing, Beiya, Tongchang, etc.; Fig. 1, Wang et al., 2018; Xu et al., 2012, 2015, 2016; Zhang and Xie, 1997; Zhang et al., 1998a, 1998b). Ages of these alkaline porphyries and associated Cu ± Mo ± Au deposits range from ~43 to 33 Ma (Hou et al., 2006; Liang et al., 2006; Xu et al., 2012). The Yulong porphyry Cu deposit is located in the northern segment of the Jinshajiang-Red river alkaline belt (Hou et al., 2003; Liang et al., 2006; Tang and Luo, 1995; Figs. 1, 2A). It is the largest porphyry Cu deposit in the Yulong porphyry Cu belt and the Jinshajiang-Red river alkaline belt.

2.2. Ore deposit geology

The ore-related intrusion of the Yulong deposit is the strongly altered monzogranite porphyry intrusion that intruded into the Triassic limestone and sandstone (T_3j Jiapila Formation and T_3b Bolila Formation, Tang and Luo, 1995; Fig. 2b). The barrel-shaped, steeply dipping Yulong monzogranite porphyry, with outcrop area of 0.64 km^2, have phenocrysts of K-feldspar, plagioclase, quartz, biotite, and amphibole, with a cryptocrystalline groundmass composed of quartz, K-feldspar, plagioclase, biotite, amphibole, and the accessory minerals mainly include titanite, apatite, zircon, and rutile (Jiang et al., 2006; Y.S. Li et al., 2012, J.X. Li etal., 2012; Xu et al., 2015, 2016). Geochemically, the Yulong monzogranite porphyry show both adakitic and shoshonitic affinities (Hou et al., 2003; Jiang et al., 2006; Xu et al., 2016; Zhang et al., 1998a, 1998b).

The pipe-like ring-shaped ore-body is characterized by inside-out alteration zoning varying from potassic, phyllic, and argillic zones (Fig. 2b; Hou et al., 2003; Tang and Luo, 1995). The barren but intensively potassic altered zone, located in the core of the ore-bearing monzogranite porphyry intrusion (Chang et al., 2017; Hou et al., 2003; Fig. 2), is characterized by pervasive formation of secondary quartz, K-feldspar, and biotite, with K-feldspar veins (Fig. 3a), biotite veins (Fig. 3b, d) and sulfide-free quartz veins (Fig. 3c) observed in this zone (Hou et al., 2003; Tang and Luo, 1995; Xu et al., 2016). The phyllic alteration zone is characterized by well-developed quartz-sulfide veins (Fig. 4), along which secondary sericite and quartz are commonly observed as alteration halos. The argillic alteration zone developed mainly in the upper and outer part of the Yulong monzogranite porphyry intrusion, which is mainly composed of kaolinite group minerals and quartz (Chang et al., 2017; Tang and Luo, 1995; Xu et al., 2016). Hornfels and skarn mineralization zones are also present in the Yulong Cu (Mo−Au) deposit, which mainly developed in the surrounding Triassic clastic rocks (Tang and Luo, 1995). The main metallic sulfides at Yulong include pyrite, chalcopyrite, molybdenite, and minor tennantite (Fig. 4). The pyrite formed in potassic alteration stage is idiomorphic and is distributed between rock-forming minerals rather than in quartz-sulfide veins (Figs. 4e, 5). No altered biotite was found to be associated with the idiomorphic pyrite. Pyrite formed at phyllic alteration stage has various occurrences including sulfide-quartz veins (Fig. 4f, g), pyrite aggregations, and pyrites coexisting with the altered biotite and amphibole (Fig. 4h).

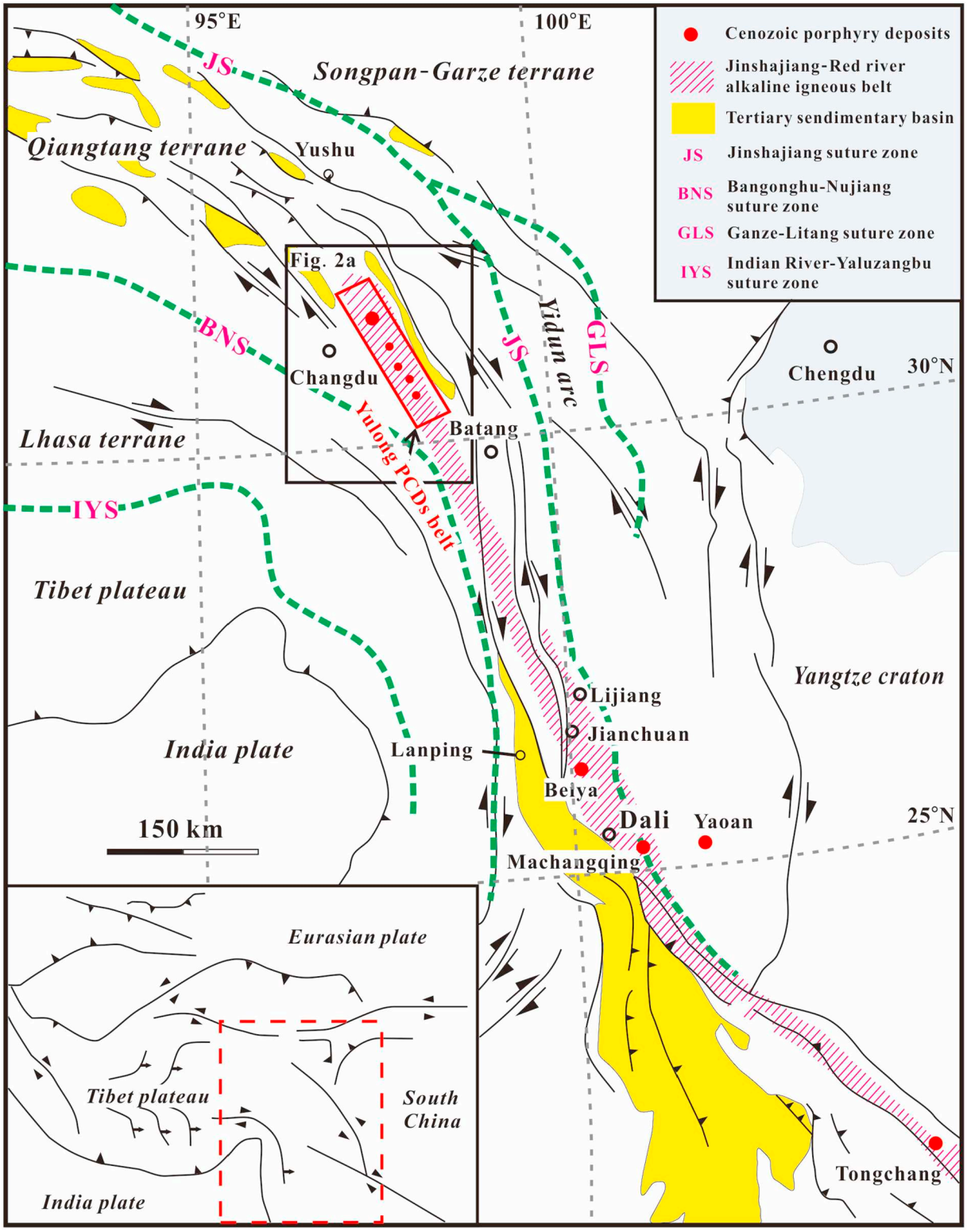

Fig. 1. Simplified geological map showing tectonic framework of the Tibetan plateau and its surrounding areas, and the spatial distribution of Cenozoic porphyry deposits in the Jinshajiang-Red River alkaline igneous belt (Modified from Wang et al., 2001). (For interpretation of the references to colour in this figure legend, the reader is referred to the web version of this article.)

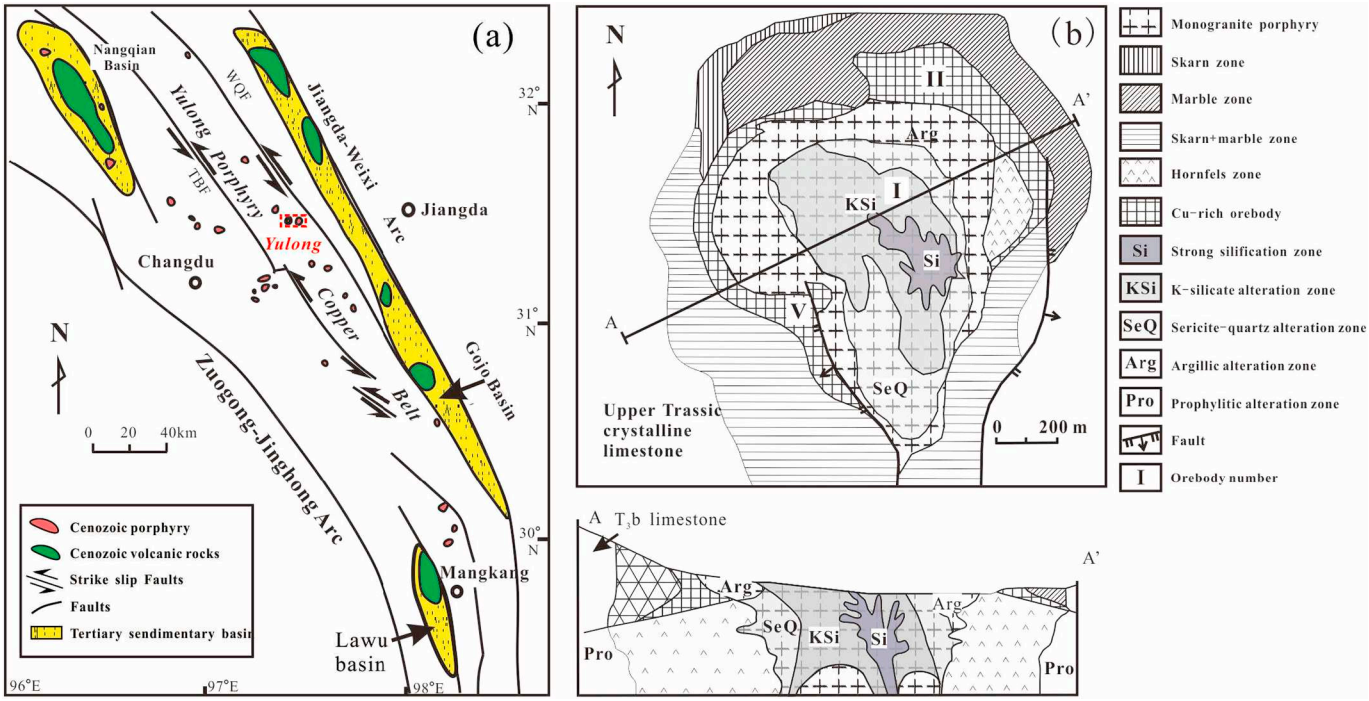

Fig. 2. (a) Simplified geological map showing distribution of ore-bearing porphyries in the Yulong porphyry Cu belt (Modified from Hou et al., 2003; Jiang et al., 2006); (b) Simplified geologic map and cross section of the Yulong porphyry Cu (Mo–Au) deposit (Modified from Hou et al., 2003; Tang and Luo, 1995).

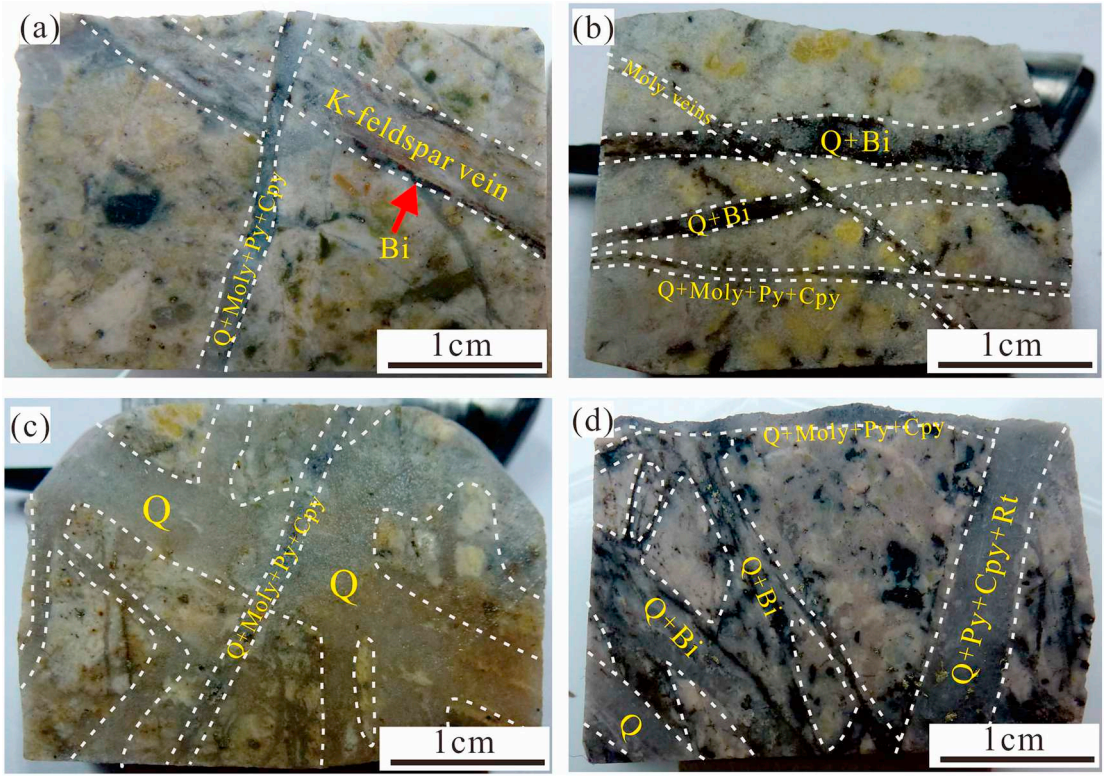

Fig. 3. Representative thin sections of potassic altered samples from the Yulong porphyry Cu deposit showing that, (a) A K-feldspar vein with biotite halo truncated by a quartz sulfide vein, (b) Q + Bi veins truncated by Q + Moly + Cpy veins, (c) Sulfide-free quartz veins, and(d) Q + Bi veins truncated by Q + Moly + Cpy veins. Abbreviations: Bi = biotite, Cpy = chalcopyrite, Kf = K-feldspar, Moly = molybdenite, Py = pyrite, Q = quartz.

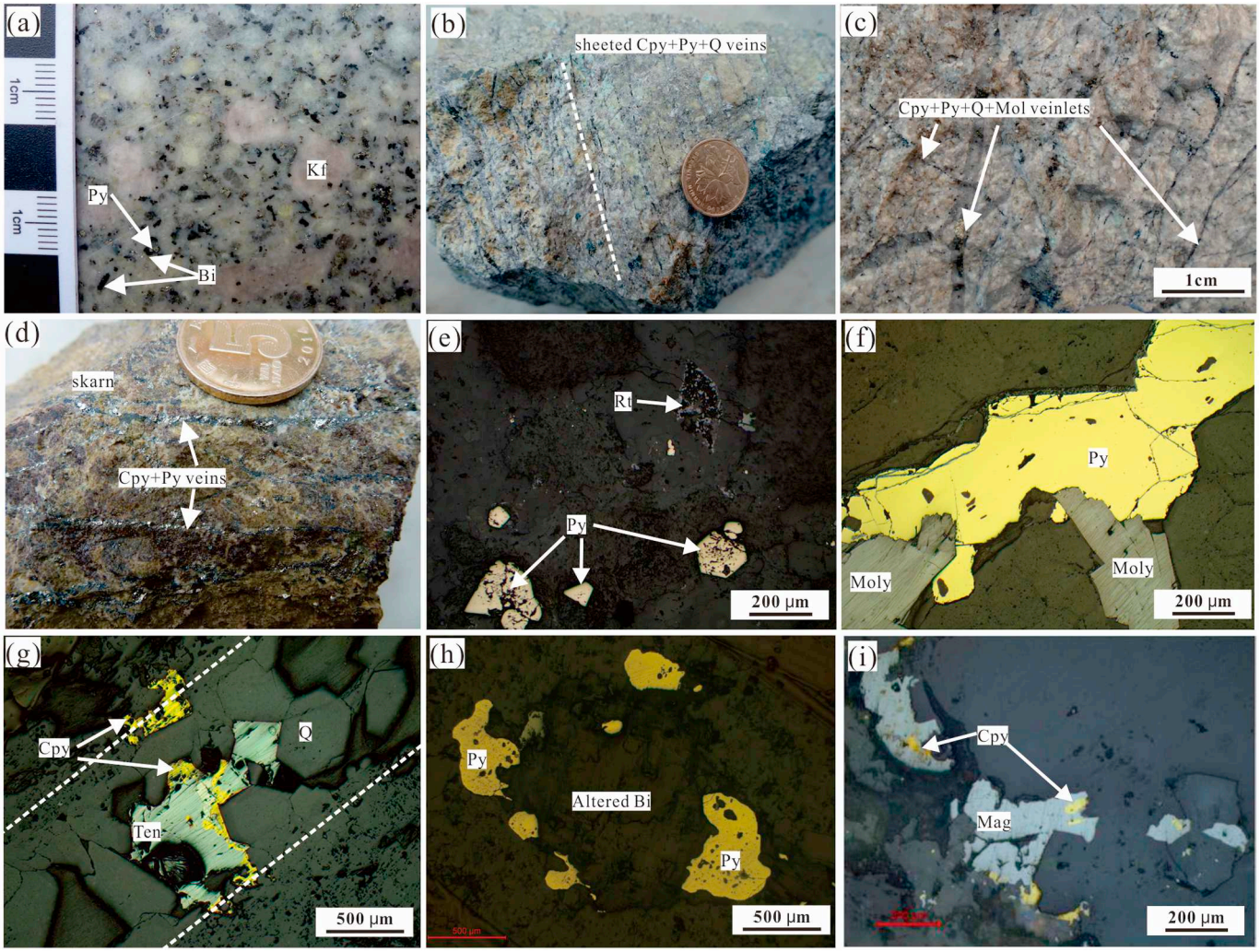

Fig. 4. (a) Porphyry ore collected from phyllic alteration zone; (b) High grade ore with sheeted Cpy + Py + Q veins; (c) High grade ore with stockwork mineralization; (d) skarn ores crosscut by sulfide veins; (e) Reflected light photograph showing idiomorphic pyrites formed in potassic alteration stage; (f) Reflected light photograph showing Q + Moly vein; (g) Reflected light photograph showing Q + Cpy + Ten vein; (h) Reflected light photograph showing Py formed aside altered Bi; (i)Co-crystallization of chalcopyrite and magnetite in the samples from phyllic alteration zone. Abbreviations: Bi = biotite, Cpy = chalcopyrite, Kf = K-feldspar, Moly = molybdenite, Py = pyrite, Q = quartz, Ten = tennantite.

3. Sampling and analytical methods

3.1. Sampling

Seventeen sulfide-bearing ore samples from phyllic alteration zone and skarn zone, where the Cu—Mo mineralization mainly occurred (Fig. 4a–c; Chang et al., 2017; Hou et al., 2003), and one sulfide-bearing sample from potassic alteration zone were collected for sulfur and lead isotopic analysis. Detailed petrographic observation was carried out on thin sections of these samples to determine the paragenesis of sulfides. Our observation shows that the sulfide minerals in the ore samples from phyllic alteration zone and skarn zone predominantly occur as quartz + sulfide veins (Fig. 4b, c, g) or sulfide veins (Fig. 4d, f). Some pyrite grains occur as aggregations beside altered biotite and amphibole (Fig. 4h). In addition, some chalcopyrite grains were also formed in close relation to magnetite (Fig. 4i). All the sulfides formed in these samples are xenomorphic in shape.

The sulfide-bearing sample from potassic alteration zone (YL1511) was overprinted by phyllic alteration to some extent. Petrographic observation reveals that it contains at least two types of pyrite (Py1 and Py2; Fig. 5). Py1 are fine- to medium-grained and appear mostly idiomorphic. They are distributed between rock-forming minerals rather than in quartz-sulfide veins, and are considered to be formed during potassic alteration stage; Py2 have various sizes ranging from fine- to coarse-grained, and usually occur as pyrite aggregation surrounding Py1. The Py2 were further replaced by tennantite as evidenced by mineralogical and textural relationships (Fig. 5). However, due to the limited sample from potassic alteration zone in this study, we cannot conclude that there are only two types of pyrites in the potassic alteration zone.

For the seventeen sulfide-bearing ore samples from phyllic alteration zone and skarn zone (see the host rocks to the sulfide minerals in Table 1), they were first crushed, and then the sulfide separates were hand-picked under a binocular microscope for sulfur and lead isotopic analysis. For one sulfide-bearing sample from the potassic alteration zone (overprinted by phyllic alteration, YL1511), in situ Nano-SIMS method was used to analyze the sulfur isotope compositions of pyrites of different generations. In addition, five least-altered ore-related monzogranite porphyry samples and six samples from surrounding wall-rocks including Triassic sandstone, limestone, and mudstone were collected for whole-rock Pb isotopic analysis.

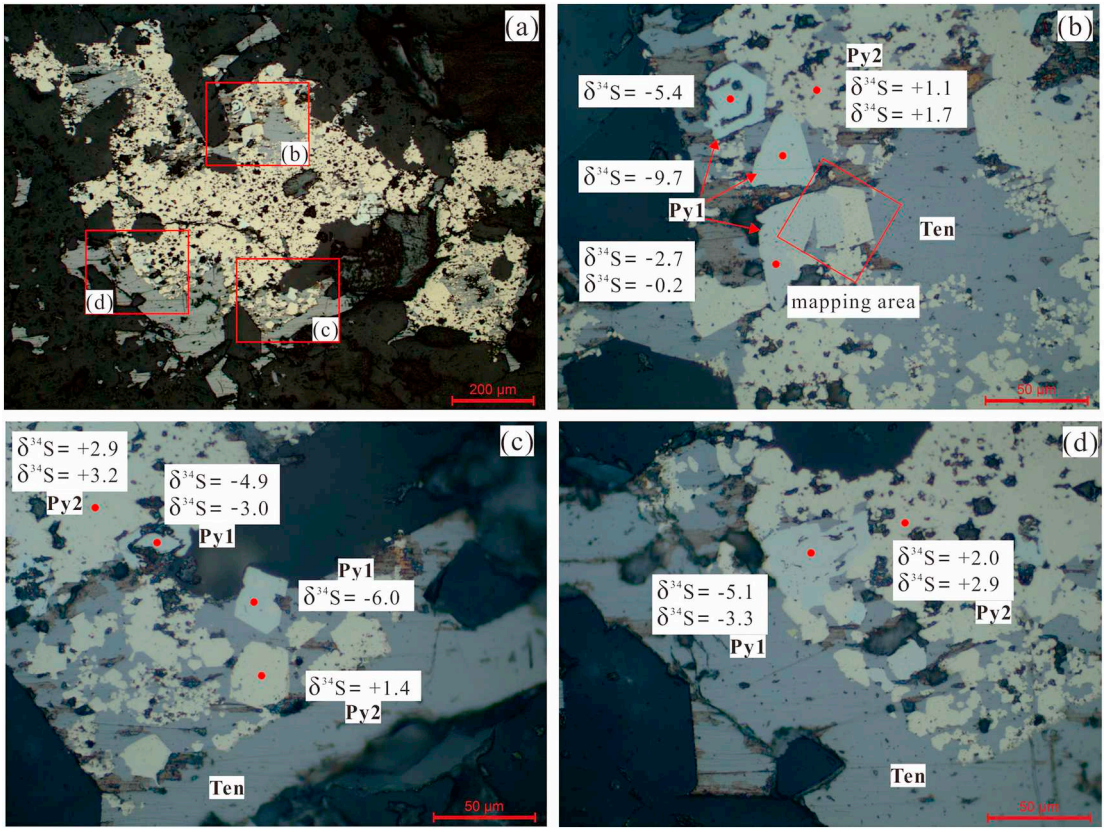

Fig. 5. Photographs showing the distribution and δ^{34} S values of Py1 and Py2 from potassic alteration zone (overprinted by phyllic alteration) of the Yulong porphyry Cu (Mo−Au) deposit. Abbreviations: Py = pyrite, Ten = tennantite.

3.2. Sulfur and Pb isotope analysis

Sulfur isotopes of sulfides were determined with a Finnigan MAT253 isotope ratio mass spectrometer at the State Key Laboratory of Ore Deposit (SKLODG), Institute of Geochemistry, Chinese Academy of Sciences (IGCAS), Guiyang, China. International reference standards of IAEA-S-1 (−0.22‰), IAEA-S-2 (22.57‰) and IAEA-S-3 (−32.53‰) are used as the external standards and Canyon Diablo Troilite (CDT) is used as the reference standard, with the analytical accuracy of ± 0.1‰ (2σ).

Chemical pretreatment of sulfide minerals and whole-rock samples used for lead isotopic analysis was carried out at the School of Earth and Space Sciences, University of Science and Technology of China, Hefei, China. About 150–200 mg sample powder was completely decomposed in a mixture of HF-$HClO_4$ at 200 °C for 7 days. Anion exchange resin (AG1-X8) was used to separate Pb. Lead isotopes were determined at SKLODG, IGCAS with Thermo Fisher Scientific Neptune Plus MC-ICP-MS. Lead standard NBS 981 was used to monitor thermal fractionation. Our routine Pb isotopic analytical results for the standard NBS 981 are $^{208}Pb/^{204}Pb = 36.692 \pm 0.001$ (2σ, n = 7), $^{207}Pb/^{204}Pb = 15.486 \pm 0.001$ (2σ, n = 7) and $^{206}Pb/^{204}Pb = 16.932 \pm 0.001$(2σ, n = 7), which are in good agreement with the recommend values (Todt et al., 1993, 1996).

In situ sulfur isotopic analysis and mapping of pyrites was conducted with Nano-SIMS at the Institute of Geology and Geophysics, Chinese Academy of Sciences (IGGCAS), Beijing, China. The prepared thin section was first cleaned and then carbon coated for in situ sulfur isotopic analysis and mapping of pyrites. Detailed operating conditions for In situ sulfur isotopic analysis and mapping of pyrites follow those described by Zhang et al. (2014). Most selected pyrite grains were analyzed twice in order to avoid accidental error.

3.3. Whole-rock trace element analysis

Trace element analysis of ore-related porphyry and wall rocks was carried out at ALS Chemex, Guangzhou, China, using a Perkin Elmer Elan 9000 inductively coupled plasma-mass spectrometer (ICP-MS). 0.200 g sample powder was mixed well with lithium metaborate flux (0.90 g) in a furnace at 1000 °C. The resultant melt was then cooled and dissolved in 100 mL of 4% HNO_3 and 2% HCl solution. Two national standards (granite GSR-1 and granitic gneiss GSR-3) were used to monitor the analytical quality. Precisions for most trace elements are better than ± 10%.

4. Analytical results

4.1. Sulfur isotopes

Sulfur isotopic results of sulfides of 17 sulfide-bearing ore samples from phyllic alteration zone and skarn zone and previously published data (Gu et al., 2003) are presented in Table 1, and sulfur isotopes of pyrites formed in potassic (Py1) and phyllic (Py2) alteration stages are presented in Table 2.

Of the sulfide minerals analyzed by MAT253, molybdenite has $\delta^{34}S$ values of +1.3 to +2.1‰ (average + 1.8‰) with an outlier of +0.5‰; pyrite has $\delta^{34}S$ values of +1.1 to +2.1‰ with an average of +1.6‰; chalcopyrite has $\delta^{34}S$ values of −0.6 to +0.5‰ with an average of −0.2‰. All the analyzed sulfides have an average $\delta^{34}S$ value of +1.1‰ (Figs. 6, 7).

In situ Nano-SIMS analysis reveals that pyrite formed in potassic alteration stage (Py1) has systematically negative $\delta^{34}S$ values of −9.7 to −0.2‰ (average = −4.5‰), whereas pyrite formed in phyllic

Table 1
$\delta^{34}S$ values of the sulfides in different types of ores from the Yulong porphyry Cu(Mo—Au) deposit ($\delta^{34}S_{V\text{-}CDT}$/‰).

Sample no.	Ore type	Py	Cpy	Moly	T (°C)	References
YL914	Porphyritic	1.1	−0.5		257	This study
YL915	Porphyritic	1.6				This study
YL916	Porphyritic	1.1	−0.6		241	This study
YL920	Porphyritic	1.8	0.5		315	This study
YL923	Porphyritic	1.6				This study
YL924	Porphyritic	1.7		2.1		This study
YL927	Porphyritic	1.7	−0.5		179	This study
YL929	Porphyritic	1.8	0.4		294	This study
YL930	Porphyritic	1.9				This study
YL935	Porphyritic	1.3	−0.5		227	This study
YL936	Porphyritic	1.4	−0.4	2.0	227	This study
YL1510	Porphyritic			1.3		This study
YL1525–7	Porphyritic	1.5				This study
YL1552–3	Porphyritic	2.1		0.5		This study
ZK44–6	Hornfels	1.1				Gu et al.,2003
YL1537–1	Hornfels	1.3		2.3		This study
ZK59–14	Hornfels	2.3				Gu et al.,2003
	Hornfels	0.1(14)				Gu et al.,2003
YL1518	Skarn	1.1				This study
YL1527	Skarn	2.0				This study
ZK1808–14	Skarn	1.4				Gu et al.,2003
ZK1808–41	Skarn	1.4				Gu et al.,2003
ZK55–9	Skarn	1.5				Gu et al.,2003
ZK51–8	Skarn	1.8				Gu et al.,2003
ZK59–10	Skarn	1.4				Gu et al.,2003
ZK32–11	Skarn	2.1				Gu et al.,2003
ZK32-W5	Skarn	2.3				Gu et al.,2003
ZK51–10	Skarn	2.4				Gu et al.,2003
ZK36–5	Skarn	2.9				Gu et al.,2003
ZK59-W1	Skarn			−1.3		Gu et al.,2003
ZK34–10	Skarn	6.0				Gu et al.,2003

T (°C) was calculated by the equation:10^3 $\ln(\delta^{34}S_{Py} - \delta^{34}S_{Cpy}) = 0.45 \times 10^6/T^2$(Ohmoto and Rye, 1979).

Table 2
$\delta^{34}S$ values of pyrites formed in potassic alteration stage (Py1) and phyllic alteration stage (Py2) from the Yulong porphyry Cu(Mo—Au) deposit.

Stage	Spot no.	$\delta^{34}S_{V\text{-}CDT}$‰	2σ
Py1	1	−5.4	0.8
	2	−9.7	0.9
	3	−2.7	0.7
	4	−0.2	0.7
	5	−6.0	0.8
	6	−4.9	0.9
	7	−3.0	0.9
	8	−5.1	0.8
	9	−3.3	0.8
Py2	1	2.0	0.7
	2	2.9	0.7
	3	1.6	0.7
	4	1.7	0.7
	5	1.1	0.7
	6	1.4	0.7
	7	3.2	0.8
	8	2.9	0.8

alteration stage (Py2) has systematically higher $\delta^{34}S$ values of +1.1 and + 3.2‰ (average = +2.1‰) (Fig. 5).

4.2. Lead isotopes

Lead isotopic compositions and analytical uncertainty of sulfides and ore-related rocks are listed in Tables 3 and 4, and are plotted in Fig. 8.

Twenty-one hand-picked sulfides samples that were previously analyzed for sulfur isotopes have $^{206}Pb/^{204}Pb$ ratios of 18.616–18.812,$^{207}Pb/^{204}Pb$ ratios of 15.670–15.740,and $^{208}Pb/^{204}Pb$ ratios of 38.956–39.067. Five least-altered whole-rock samples from the ore-related porphyries have $^{206}Pb/^{204}Pb$ ratios of 18.783–18.885,$^{207}Pb/^{204}Pb$ ratios of 15.661–15.668,and $^{208}Pb/^{204}Pb$ ratios of 38.992–39.010. Six fresh whole-rock samples from the ore-hosting sedimentary rocks have $^{206}Pb/^{204}Pb$ ratios of 18.731–19.028,$^{207}Pb/^{204}Pb$ ratios of 15.656–15.719,and $^{208}Pb/^{204}Pb$ ratios of 38.940–39.252. Initial Pb isotopic compositions of the ore-related porphyries and ore-hosting sedimentary rocks were calculated based on the whole-rock Pb isotopic ratios, and U, Th and Pb contents, and mineralization age (~41 Ma; Chang et al., 2017; Hou et al., 2006; Tang et al., 2009). Calculated initial Pb isotopic results show that the ore-related porphyries have $(^{206}Pb/^{204}Pb)_i$ of 18.549–18.718, $(^{207}Pb/^{204}Pb)_i$ of 15.647–15.662, and $(^{208}Pb/^{204}Pb)_i$ ratios of 38.794–38.888, and the ore-hosting sedimentary rocks have $(^{206}Pb/^{204}Pb)_i$ of 18.423–18.761, $(^{207}Pb/^{204}Pb)_i$ of 15.654–15.713, and $(^{208}Pb/^{204}Pb)_i$ ratios of 38.867–39.062.

5. Discussion

5.1. Sulfur sources

Sulfides crystallized under highly oxidized fluid environments will have sulfur isotopic compositions remarkably different from their parental fluids (Ohmoto, 1972). A case study of this would be the Butte porphyry Cu—Mo deposit in USA. At Butte, the sulfide $\delta^{34}S$ values (+1.0 to +2.0‰) suggest a magmatic origin of the sulfur; however, the high modal mineral ratios of sulfate/sulfide (Fig. 7) indicate that the $\delta^{34}S_{\Sigma S}$ values of the ore-forming fluids were heavy ($\delta^{34}S_{\Sigma S}$ = ~ +10‰), and an evaporitic crustal component was proposed to have contributed sulfur to the ore-forming fluids (Field et al., 2005). In addition, the Far Southeast porphyry Cu—Au deposit and Ampucao porphyry Cu—Au deposit in Philippine also have elevated $\delta^{34}S_{\Sigma S}$ values than the normal magmatic sulfur (Fig. 7). They were interpreted to represent a seawater sulfur contribution to the hydrothermal fluids (Sasaki et al., 1984). These studies suggest that the sulfide $\delta^{34}S$ values alone should be used with care when indicating the sulfur sources.

At Yulong, anhydrite was found to occur as daughter mineral in the primary fluid inclusion in quartz phenocryst of the ore-related monzogranite porphyry (Liang et al., 2009). Nonetheless, the absence of sulfates coexisting with abundant sulfides in ores suggests that the ore-forming fluids responsible for metal deposition at Yulong are primarily reduced, with S^{2-} being the main sulfur species (Ohmoto, 1972). Therefore, the $\delta^{34}S$ values of sulfides can approximately represent the $\delta^{34}S$ value of bulk fluid (Ohmoto and Rye, 1979; Yang, 2012). The sulfides from Yulong have uniform and near zero $\delta^{34}S$ values ($\delta^{34}S$ = −1.3 ~ +2.9‰, average + 1.2‰; Figs. 6, 7; Table 1), indicating a magmatic origin of the sulfur ($\delta^{34}S$ = 0 ± 3‰; Chaussidon et al., 1989).

In situ Nano-SIMS analysis revealed that pyrite formed in potassic alteration stage (Py1) have negative $\delta^{34}S$ values ($\delta^{34}S$ = −9.7 to −0.2‰, average = −4.5‰; Figs. 5, 6). These values are different from the sulfur isotope values of sulfide minerals analyzed by a conventional method (Fig. 6; Gu et al., 2003). We consider that this is because these sulfide minerals were formed at different alteration stages. The pyrite analyzed by Nano-SIMS was formed during the potassic alteration stage, whereas the sulfide minerals analyzed by a conventional method (Fig. 6; Gu et al., 2003) were formed in the phyllic alteration stage. During the potassic alteration stage, the SO_2 dissolved in the ore-forming fluids progressively disproportionate to H_2S and H_2SO_4 as the fluids cools to < 400 °C(Richards, 2011; Rye, 1993; Seal, 2006):

$$4SO_2 + 4H_2O = H_2S + 3H_2SO_4 \quad (1)$$

The resultant H_2S initiates precipitation of sulfides in the potassic alteration stage. Due to the equilibrium with sulfate minerals, the resultant sulfides in this stage would have relatively low and negative $\delta^{34}S$ values. Pyrites formed during the phyllic alteration stage (Py2)

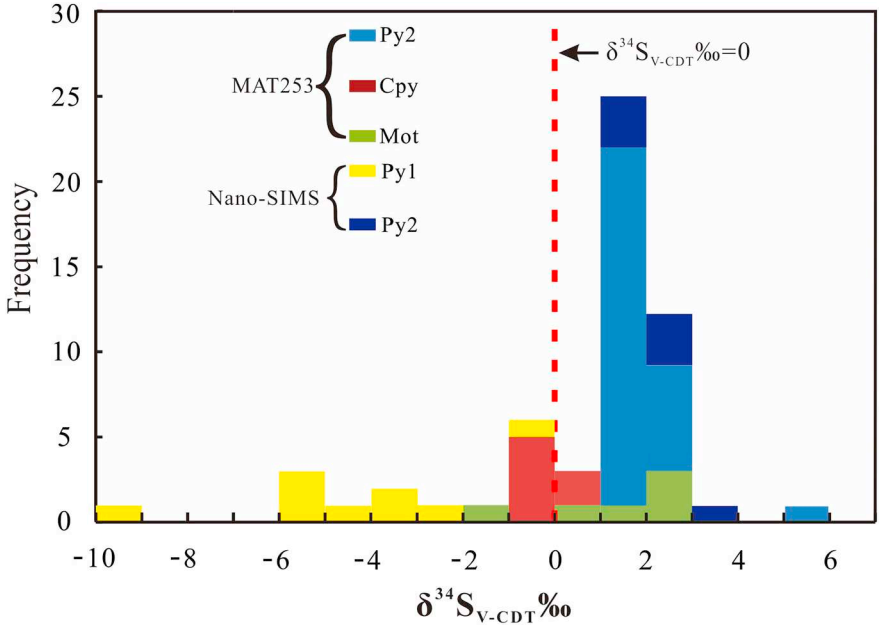

Fig. 6. Histogram of δ^{34} S values for sulfides from the Yulong porphyry Cu deposit.

have uniform positive $\delta^{34}S$ values ($\delta^{34}S$ = +1.1 to +3.2‰, ave. +2.1‰; Figs. 5, 6; Table 2), which are similar to sulfide minerals analyzed by conventional method. We attribute this to reservoir effect due to reduction of the preformed SO_4^{2-} [Eq. (1)], which was probably promoted by magnetite crystallization (Liang et al., 2009).

$$12FeO + H_2SO_4 = 4Fe_3O_4 + H_2S \quad (2)$$

This reaction [Eq. (2)] is reflects the co-crystallization of chalcopyrite with magnetite at Yulong (Fig. 4i). The reduction and consumption of the SO_4^{2-} with relatively higher $\delta^{34}S$ values would gradually increase the $\delta^{34}S$ values of the sulfides formed afterwards. Similar situations also have been reported in other porphyry or porphyry-like deposits (e.g., porphyry-epithermal Cu—Au deposits in Baguio district, Philippines, Cooke et al., 2011; Wangjiazhuang Cu—Mo deposit, north China, Lan et al., 2017). Therefore the disproportionation of aqueous SO_2 and subsequent sulfate reduction processes further suggest the magmatic origin of the sulfur.

5.2. Lead sources

Similar to the post-Eocene porphyry Cu ± Mo ± Au deposit systems in the Andes belt (Chiaradia, 2004; Cooke et al., 2014), sulfide minerals from ores of the Yulong deposit have initial Pb isotopic compositions deviating from those of the spatially and genetically related monzogranite porphyry, but more close to those of the ore-hosting strata (Fig. 8a–b). This allows the interpretation that both ore-related monzogranite porphyry and ore-hosting strata have provided ore-forming materials (e.g., Pb) for the Yulong porphyry Cu (Mo—Au) deposit. The Pb isotopic compositions of the country rocks present a range of compositions at 41 Ma. A few sulfide minerals have higher Pb isotopic compositions than the country rocks and porphyry intrusion (Fig. 8a). This might have resulted from another source of Pb other than the ore-related porphyry and the ore-hosting strata. Nonetheless, the sulfides have initial Pb isotopic compositions that mainly overlap those of the ore-hosting strata, suggesting a significant amount of the Pb budget was provided by the ore-hosting strata.

Previous studies about post-subduction porphyry Cu-Mo-Au deposits generally suggest identical sources of Pb between sulfides and ore-bearing porphyries (Qulong, Jiama, Nanmu and Chongjiang in Gangdese belt, Southern Tibet, Meng et al., 2006; Qu et al., 2002; The giant Beiya porphyry-skarn Au-polymetallic deposit, SW China, He, 2014) or insignificant contributions from external sources in the late stage sulfides (e.g. Porphyry Cu deposits in the Kerman belt, SE Iran, Shafiei, 2010). Therefore this study represents a case in which ore-hosting strata have significantly contributed to the ore-forming materials in post-subduction porphyry deposit systems. Furthermore, our study reinforces the conclusion of Cooke et al. (2014) that Pb isotope compositions of the ore-minerals in porphyry Cu deposits could be strongly influenced by the wall-rocks that were encountered during hydrothermal circulation, and that fluid-rock interaction is probably a normal process in porphyry-type mineralization.

5.3. Implication for metal precipitation

$\delta^{34}S$ values of sulfides from phyllic alteration zones of Yulong porphyry Cu (Mo—Au) deposit in this study increase regularly from chalcopyrite to pyrite and then to molybdenite. This is best shown in sample YL936 where these minerals co-exist (Table 1). Such regular variations in $\delta^{34}S$ values probably indicate equilibrium fractionation of S isotopes between different sulfide phases in the magmatic-hydrothermal system (Ohmoto and Rye, 1979; Zheng and Chen, 2000). Therefore, $\delta^{34}S$ values of different mineral pairs could be used to constrain the ore-formation temperatures based on sulfur isotope thermometry studies compiled by Ohmoto and Rye (1979).

Seven pyrite-chalcopyrite pairs yielded equilibrium temperatures of 179° to 315 °C (average = 245 °C). These temperatures are consistent with published homogenization temperature data of fluid inclusions of the argillic alteration stage, but lower than the fluid inclusion homogenization temperatures of phyllic and potassic alteration stages (Gu et al., 2003; Hou et al., 2007; Li et al., 1981; Wang et al., 2018). In addition, these calculated temperatures are also lower than the temperatures of Cu—Fe sulfides precipitation in porphyry systems (> 300 °C; Hemley et al., 1992; Klemmet al., 2007; Landtwing et al., 2005). This probably suggests re-equilibration during later, lower temperature alteration (intermediate argillic stage < 300 °C). Nano-SIMS mapping, together with the microscope observation, show that Py2 (phyllic alteration stage) contain much higher concentrations of Au and As than Py1 (potassic alteration stage; Figs. 4g, 9), suggesting that Au mineralization, which is closely related to As-rich fluids, mainly occurred in the phyllic alteration stage. The tight relation between Au

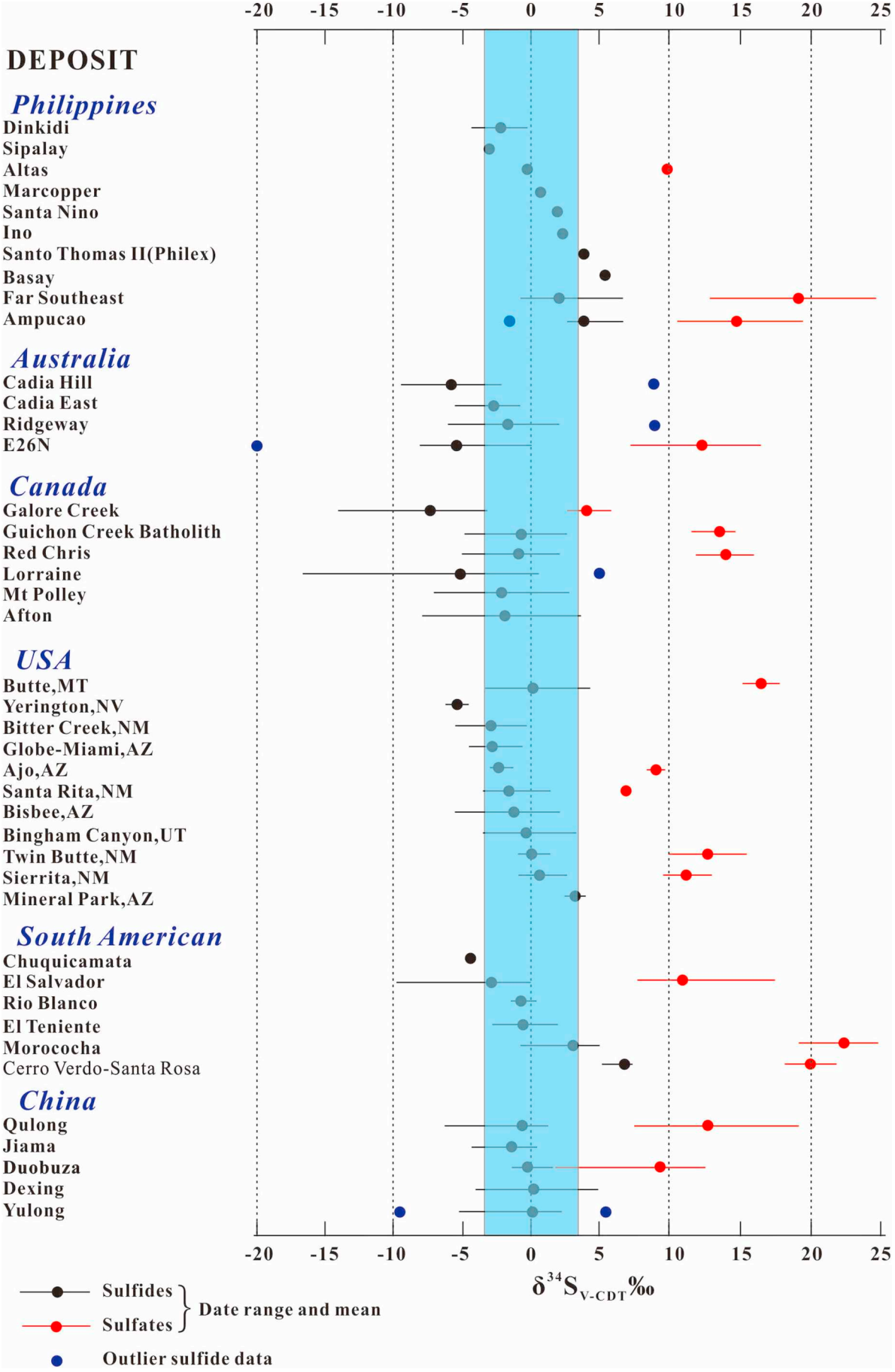

(caption on next page)

Fig. 7. δ^{34} S values for sulfides and sulfates from selected porphyry Cu deposits around the world (Modified from Cooke et al., 2014; Wilson et al., 2007). Data of the Yulong deposit are from Table 1; data of the Qulong deposit are from Qin et al. (2014) and Qu et al. (2002); data of the Jiama deposit are from Y.S. Li et al., 2012 and Zheng (2017); data of the Duobuza deposit are from He et al. (2016); data of the Dexing deposit are from Zhou et al. (2012) and references therein; data of other deposits are from Cooke et al. (2014) and references therein.

mineralization and the As-rich fluids was also reported in other porphyry-epithermal Cu−Au deposits (e.g., the Yanacocha and Pueblo Viejo high-sulfidation epithermal Au deposits, Deditius et al., 2009; The giant Dexing porphyry Cu−Au deposit, China, Reich et al., 2013). The above-mentioned studies reveal that large-scaled precipitation of ore-forming metals Cu, Mo, and Au at Yulong occurred in the phyllic alteration stage with temperatures of > 300 °C.

5.4. Implication for magmatic-hydrothermal process

The discrepancy between porphyry and sulfide Pb isotopes could also put constraints on the ore-forming process at Yulong. The high-temperature magma genesis process will ultimately homogenize the Pb isotope of the magma and the rocks the magma assimilated when rising to shallow crust (Cooke et al., 2014). Therefore, the hydrothermal fluids derived from the homogenized magma are expected to have the same Pb isotopic composition as the magma. As such, the discrepancy between porphyry and sulfide Pb isotopes indicates that the incorporation of wall-rock Pb occurred after the exsolution of the magmatic fluid. Furthermore, the narrow range of sulfide Pb isotopes indicates that the ore-forming fluids were isotopically homogeneous, which further suggests the mixing of porphyry- and wall-rock derived Pb must have happened prior to ore deposition (e.g., Dilles et al., 1995; Force, 1998; Mukasa et al., 1990; Tosdal et al., 1999). But nonetheless, further work would be needed to see if there is a change of Pb isotopes from the potassic zone to phyllic zone.

Fluid-wall rock interaction during the ascent of magmatic fluids has been proposed to be responsible for the mixed Pb isotope features of sulfide minerals in porphyry Cu systems (Bouse et al., 1999; Richards et al., 1991; Tosdal and Munizaga, 2003). During ascent, the magmatically derived fluids reacted with the country rocks (Richards et al., 1991), scavenged the radiogenic Pb from these rocks and then became homogenous due to high temperature mixing. The radiogenic Pb was finally incorporated into the sulfide minerals.

Table 3
Lead isotopic compositions of sulfides, ore-related porphyries, feldspar from ore-related porphyries, and ore-hosting strata for the Yulong porphyry Cu (Mo−Au) deposit.

Sample	Mineral/rock	$^{206}Pb/^{204}Pb$	± 2σ	$^{207}Pb/^{204}Pb$	± 2σ	$^{208}Pb/^{204}Pb$	± 2σ	Data sources
YL914	Pyrite	18.755	0.003	15.696	0.003	39.053	0.007	This study
YL914	Chalcopyrite	18.755	0.002	15.693	0.002	39.046	0.006	
YL915	Pyrite	18.730	0.003	15.670	0.003	38.967	0.008	
YL916	Pyrite	18.691	0.002	15.725	0.002	39.025	0.004	
YL920	Pyrite	18.750	0.002	15.697	0.002	39.050	0.004	
YL920	Chalcopyrite	18.753	0.002	15.690	0.002	39.052	0.005	
YL923	Pyrite	18.716	0.002	15.700	0.002	39.009	0.005	
YL924	Pyrite	18.705	0.003	15.712	0.002	39.016	0.006	
YL927	Pyrite	18.616	0.002	15.740	0.002	38.956	0.004	
YL927	Chalcopyrite	18.630	0.003	15.736	0.003	38.980	0.008	
YL929	Pyrite	18.750	0.002	15.696	0.002	39.045	0.006	
YL929	Chalcopyrite	18.737	0.003	15.685	0.003	39.002	0.008	
YL930	Pyrite	18.742	0.007	15.683	0.006	39.010	0.014	
YL935	Pyrite	18.750	0.002	15.687	0.002	39.023	0.004	
YL935	Chalcopyrite	18.771	0.004	15.693	0.004	39.053	0.009	
YL936	Pyrite	18.694	0.002	15.708	0.002	38.996	0.005	
YL936	Chalcopyrite	18.673	0.004	15.721	0.003	38.999	0.009	
YL1518	Pyrite	18.731	0.004	15.689	0.004	38.986	0.005	
YL1525–7	Pyrite	18.812	0.005	15.719	0.004	39.067	0.010	
YL1537–1	Pyrite	18.755	0.006	15.706	0.005	39.045	0.011	
YL1552–3	Pyrite	18.733	0.003	15.683	0.002	39.004	0.013	
YL909	Monzogranite porphyry	18.707	0.003	15.656	0.003	38.888	0.007	This study
YL919	Monzogranite porphyry	18.718	0.003	15.658	0.003	38.887	0.008	
YL1525–7	Monzogranite porphyry	18.682	0.005	15.658	0.005	38.794	0.014	
YL1528–1	Monzogranite porphyry	18.703	0.005	15.662	0.004	38.864	0.012	
YL1528–2	Monzogranite porphyry	18.549	0.004	15.647	0.003	38.800	0.009	
YL-J-1	Feldspar	18.714	0.006	15.658	0.006	38.895	0.014	Jiang et al.,2006
YL-J-2	Feldspar	18.751	0.008	15.673	0.010	38.963	0.034	
YL-J-3	Feldspar	18.736	0.006	15.661	0.006	38.937	0.018	
YL-J-4	Feldspar	18.713	0.006	15.646	0.006	38.867	0.022	
YL-J-5	Feldspar	18.824	0.006	15.665	0.004	38.999	0.012	
YL-J-6	Feldspar	18.731	0.016	15.661	0.020	38.924	0.066	
YL-J-7	Feldspar	18.718	0.014	15.652	0.012	38.895	0.028	
YL-J-8	Feldspar	18.720	0.008	15.654	0.006	38.894	0.016	
YL-J-9	Feldspar	18.718	0.008	15.646	0.008	38.874	0.018	
YL-J-10	Feldspar	18.735	0.006	15.663	0.004	38.933	0.012	
YL1526	Marble	18.761	0.001	15.672	0.001	38.985	0.004	This study
YL1537–2	Sandstone	18.696	0.001	15.691	0.001	38.977	0.003	
YL1541–2	Sandstone	18.423	0.002	15.669	0.001	38.906	0.004	
YL1554	Mudstone	18.553	0.001	15.654	0.001	38.867	0.003	
YL1555	Marble	18.726	0.001	15.664	0.001	38.935	0.002	
ZK1213–390	Mudstone	18.731	0.001	15.713	0.001	39.062	0.003	

Table 4
Caculated initial Pb isotopic compositions of ore-related porphyries and ore-hosting strata for the Yulong porphyry Cu (Mo−Au) deposit.

Sample	Rock type	$^{206}Pb/^{204}Pb$	$^{207}Pb/^{204}Pb$	$^{208}Pb/^{204}Pb$	Pb (ppm)	Th (ppm)	U (ppm)	t (Ma)	$(^{206}Pb/^{204}Pb)_i$	$(^{207}Pb/^{204}Pb)_i$	$(^{208}Pb/^{204}Pb)_i$
YL909	Monzogranite porphyry	18.837	15.662	39.009	23.3	20.8	7.4	41	18.707	15.656	38.888
YL919	Monzogranite porphyry	18.783	15.661	38.992	20.7	16.1	3.3	41	18.718	15.658	38.887
YL1525–7	Monzogranite porphyry	18.837	15.665	38.995	15.1	22.5	5.7	41	18.682	15.658	38.794
YL1528–1	Monzogranite porphyry	18.821	15.668	38.997	27.1	26.6	7.8	41	18.703	15.662	38.864
YL1528–2	Monzogranite porphyry	18.885	15.663	39.010	15.8	24.5	12.9	41	18.549	15.647	38.800
YL1526	Marble	18.843	15.675	39.089	13.2	10.1	2.63	41	18.761	15.672	38.985
YL1537–2	Sandstone	18.836	15.698	39.088	11.5	9.39	3.91	41	18.696	15.691	38.977
YL1541–2	Sandstone	19.028	15.697	39.252	3.63	9.17	5.31	41	18.423	15.669	38.906
YL1554	Mudstone	18.598	15.656	38.943	28	15.6	3.11	41	18.553	15.654	38.867
YL1555	Marble	18.731	15.664	38.940	149	4.91	1.83	41	18.726	15.664	38.935
ZK1213–390	Mudstone	18.850	15.719	39.178	11.3	9.66	3.26	41	18.731	15.713	39.062

Note: $^{206}Pb/^{204}Pb$, $^{207}Pb/^{204}Pb$ and $^{208}Pb/^{204}Pb$ represent the analytical values, $(^{206}Pb/^{204}Pb)_i$, $(^{207}Pb/^{204}Pb)_i$ and $(^{208}Pb/^{204}Pb)_i$ represent the initial values calculated back to 41 Ma using the computer program of Lu (2004) and the listed concentrations of U, Th and Pb; t (Ma) represent the age of Monzogranite porphyry. The decay constant values of 1.55125×10^{-10} for ^{238}U, 9.8485×10^{-10} for ^{235}U and 4.9475×10^{-11} for ^{232}Th were used (Steiger and Jäger, 1977).

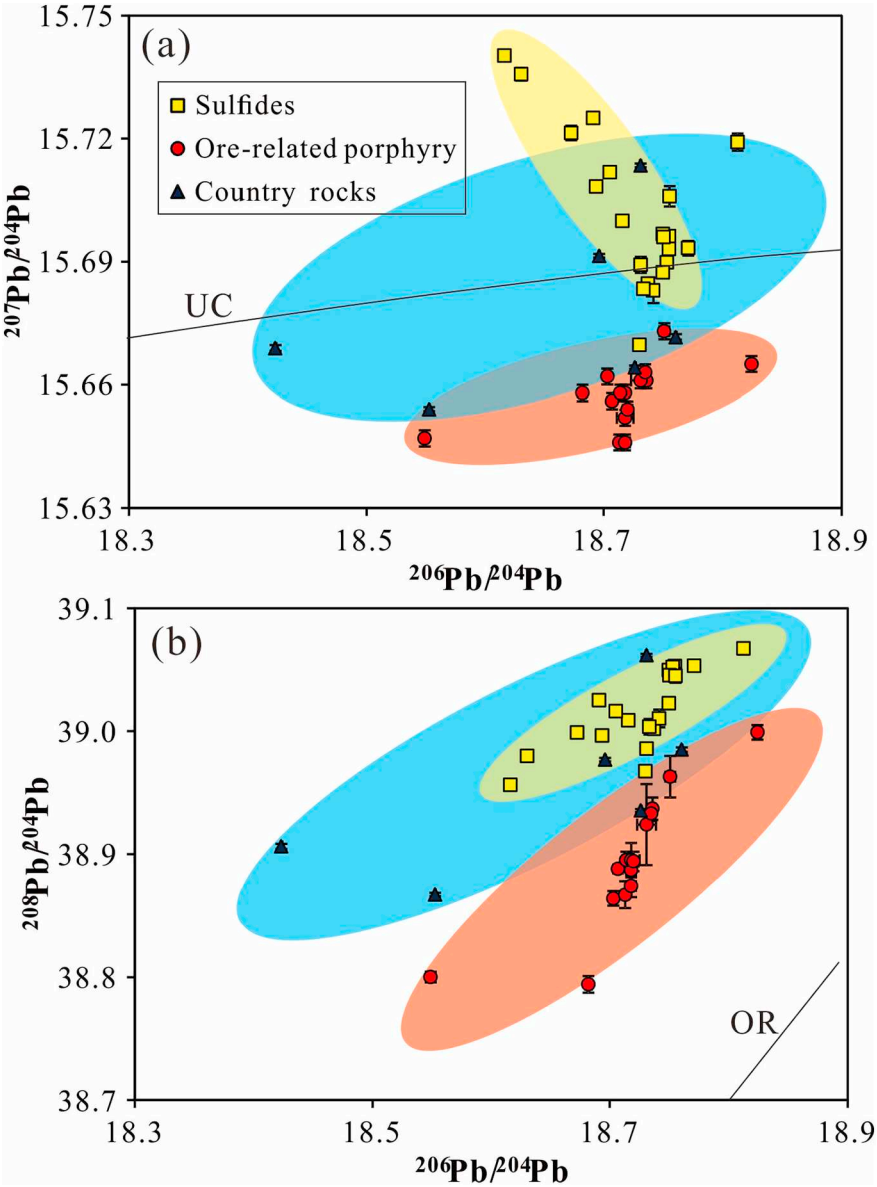

Fig. 8. (a) $(^{207}Pb/^{204}Pb)_i$ vs $(^{206}Pb/^{204}Pb)_i$, and (b) $(^{208}Pb/^{204}Pb)_i$ vs $(^{206}Pb/^{204}Pb)_i$ plots of sulfides, ore-related porphyries and ore-hosting strata for the Yulong porphyry Cu(Mo−Au) deposit. The upper-crust (UC) and orogen (OR) evolution curves are from Zartman and Doe (1981). All data are provided in Tables 2 and 3.

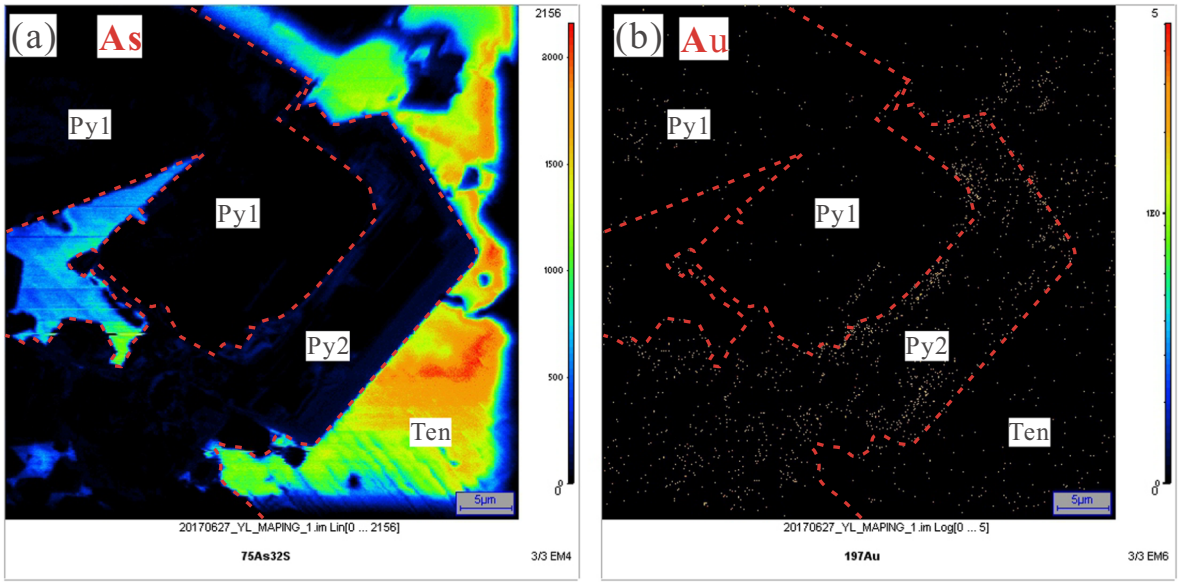

Fig. 9. Nano-SIMS mapping of Py1 and Py2 (location shown in Fig. 5b) from the Yulong porphyry Cu (Mo−Au) deposit, showing the relatively high As and Au contents in Py2. Abbreviations: Py = pyrite, Ten = tennantite.

6. Conclusions

1. Uniform sulfur isotopic compositions of sulfides suggest a magmatic origin of the sulfur at the Yulong deposit. In situ Nano-SIMS analysis further reveals that pyrite formed in the potassic alteration stage have systematically negative $\delta^{34}S$ values, whereas pyrite formed in the phyllic alteration stage have systematically positive $\delta^{34}S$ values; This regular variation is considered to have resulted from disproportionation of aqueous SO_2 and subsequent reduction of SO_4^{2-}.
2. Pb isotopic compositions suggest that Pb of ores was provided by both the ore-related porphyry and ore-hosting strata. Mixing of porphyry- and wall-rock Pb was probably caused by fluid-wall rock interaction during fluid ascent.
3. Sulfur isotope geothermometry and Nano-SIMS mapping, together with published homogenization temperature data of fluid inclusions, reveal that large-scale precipitation of ore-forming metals (e.g., Cu, Mo and Au) primarily occurred at temperatures > 300 °C.

Acknowledgements

This study is jointly supported by the Strategic Priority Research Program (B) of the Chinese Academy of Sciences (XDB18000000), the CAS/SAFEA International Program for Creative Research Teams, the Natural Science Foundations of China (41873052, 41473052), and the National Basic Research Program (2015CB452603). Xiang-Yuan Sheng, He-Qing Liu and staff of Nano-SIMS laboratory of IGGCAS are thanked for the help of In situ sulfur analysis. Kind help with the chemical pretreatment of Pb isotope analysis from Ping Xiao (University of Science and Technology of China) is gratefully acknowledged. We are grateful to Dr. Xue-Ming Yang, Richard M. Tosdal, and an anonymous reviewer for their constructive and valuable reviews. Editor-in-Chief Robert Ayuso and associate editor David R. Lentz are thanked for their valuable suggestions and efforts in handling the manuscript.

References

Bi, X.W., Hu, R.Z., Cornell, D.H., 2002. The origin of altered fluid: REE evidence from primary and secondary feldspars in the mineralization zone. Ore Geol. Rev. 19, 69–78.
Bi, X.W., Hu, R.Z., Cornell, D.H., 2004. The alkaline porphyry associated Yao'an gold deposit, Yunnan, China: rare earth element and stable isotope evidence for magmatic hydrothermal ore formation. Mineral. Deposita 39 (1), 21–30.
Bi, X.W., Hu, R.Z., Peng, J.T., Wu, K.X., Su, W.C., Zhang, X.Z., 2005. Geochemical characteristics of the Yao'an and Machangqing alkaline-rich intrusions. Acta Petrol. Sin. 21 (01), 0113–0124 (in Chinese).
Bi, X.W., Hu, R.Z., Hanley, J.J., Mungall, J.E., Peng, J.T., Shang, L.B., Wu, K.X., Shuang, Y., Li, H.L., Hu, X.Y., 2009. Crystallization conditions (T, P, fO_2) from mineral chemistry of Cu- and Au-mineralized alkaline intrusions in the Red River–Jinshajiang alkaline igneous belt, western Yunnan Province, China. Mineral. Petrol. 96, 43–58.
Bouse, R.M., Ruiz, J., Titley, S.R., Tosdal, R.M., Wooden, J.L., 1999. Lead isotope compositions of late cretaceous and early tertiary igneous rocks and sulfide minerals in Arizona; implications for the sources of plutons and metals in porphyry copper deposits. Econ. Geol. Bull. Soc. Econ. Geol. 94 (2), 211–244.
Chang, J., Li, J.W., Selby, D., Liu, J.C., Deng, X.D., 2017. Geological and chronological constraints on the long-lived Eocene Yulong porphyry Cu-Mo deposit, eastern Tibet, China: implications for lifespan of magmatic-hydrothermal processes forming giant and supergiant porphyry Cu deposits. Econ. Geol. 112 (7), 1719–1746.
Chaussidon, M., Albarede, F., Sheppard, S.M.F., 1989. Sulphur isotope variations in the mantle from ion microprobe analyses of micro-sulphide inclusions. Earth Planet. Sci. Lett. 92, 144–156.
Chiaradia, M., 2004. Metal sources in mineral deposits and crustal rocks of Ecuador (1°N-4°S): a lead isotope synthesis. Econ. Geol. 99 (6), 1085–1106.
Cooke, D.R., Hollings, P., Walshe, J.L., 2005. Giant porphyry deposits: characteristics, distribution, and tectonic controls. Econ. Geol. 100 (5), 801–818.
Cooke, D.R., Deyell, C.L., Waters, P.J., Gonzales, R.I., Zaw, K., 2011. Evidence for magmatic-hydrothermal fluids and ore-forming processes in epithermal and porphyry deposits of the Baguio district, Philippines. Econ. Geol. 106 (8), 1399–1424.
Cooke, D.R., Hollings, P., Wilkinson, J.J., Tosdal, R.M., 2014. Geochemistry of porphyry deposits. In: Holland, H.D., Turekian, K.K. (Eds.), Treatise on Geochemistry, Second edition. 13. Elsevier, Oxford, pp. 357–381.
Deditius, A., Utsunomiya, S., Ewing, R.C., Chryssoulis, S.L., Venter, D., Kesler, S.E., 2009. Decoupled geochemical behavior of As and Cu in hydrothermal systems. Geology 37, 707–710.
Dilles, J.H., Farmer, G.L., Field, C.W., 1995. Sodium-calcium alteration by non-magmatic saline fluids in porphyry copper deposits: results from Yerington, Nevada. In: Mineralogical Association of Canada Short Course Handbook. 23. pp. 309–338.
Field, C.W., Zhang, L., Dilles, J.H., Rye, R.O., Reed, M.H., 2005. Sulfur and oxygen isotopic record in sulfate and sulfide minerals of early, deep, pre-main stage porphyry Cu–Mo and late main stage base-metal mineral deposits, butte district, Montana. Chem. Geol. 215 (1), 61–93.
Force, E.G., 1998. Laramide alteration of Proterozoic diabase: a likely contributor to porphyry systems in the Dripping Spring Mountains area, southeastern Arizona. Econ. Geol. 93, 171–183.
Gu, X.X., Tang, J.X., Wang, C.S., Chen, J.P., He, B.B., 2003. Himalayan magmatism and porphyry copper–molybdenum mineralization in the Yulong ore belt, east Tibet. Mineral. Petrol. 78 (1–2), 1–20.
Guo, L.G., Liu, Y.P., Xu, W., Zhang, X.C., Qin, K.Z., Li, T.S., Shi, Y.R., 2006. Constraints to the mineralization age of the Yulong porphyry copper deposit from SHRIMP U–Pb zircon data in Tibet. Acta Petrol. Sin. 22, 1009–1016 (in Chinese with English abstract).
He, W.Y., 2014. The Beiya Giant Gold-polymetallic Deposit: Magmatism and Metallogenic Model (PhD thesis). China University of Geosciences, Beijing (in Chinese).
He, Y.Y., Wen, C.Q., Liu, X.F., 2016. Sulfur and lead isotope geochemical tracing of the Duobuza copper deposit, Tibet. In: Acta Petrologica Et Mineralogica, (in Chinese with English abstract).

Hemley, J.J., Cygan, G.L., Fein, J.B., Robinson, G.R., D'Angelo, W.M., 1992. Hydrothermal ore-forming processes in the light of studies in rock-buffered systems: I. Iron–copper–zinc–lead sulfide solubility relations. Econ. Geol. 87, 1–22.
Hou, Z.Q., Ma, H.W., Zaw, K., Zhang, Y.Q., Wang, M.J., Wang, Z., Pan, G.T., Tang, R.L., 2003. The Himalayan Yulong porphyry copper belt: product of large-scale strike-slip faulting in eastern Tibet. Econ. Geol. 98, 125–145.
Hou, Z.Q., Zeng, P.S., Gao, Y.F., Du, A.D., Fu, D.M., 2006. Himalayan Cu–Mo–Au mineralization in the eastern Indo–Asian collision zone: constraints from Re–Os dating of molybdenite. Mineral. Deposita 41, 33–45.
Hou, Z.Q., Xie, Y.L., Xu, W.Y., Li, Y.Q., Zhu, X.K., Khin, Z., Beaudoin, G., Rui, Z.Y., Huang, W., Luobu, C.R., 2007. Yulong deposit, eastern Tibet: a high-sulfidation Cu-Au porphyry copper deposit in the eastern Indo-Asian collision zone. Int. Geol. Rev. 49 (3), 235–258.
Hou, Z.Q., Yang, Z.M., Qu, X.M., Meng, X.J., Li, Z.Q., Beaudoin, G., Rui, Z.Y., Gao, Y.F., Zaw, K., 2009. The Miocene Gangdese porphyry copper belt generated during post-collisional extension in the Tibetan orogen. Ore Geol. Rev. 36, 25–51.
Hou, Z.Q., Zhang, H.R., Pan, X.F., Yang, Z.M., 2011. Porphyry Cu (–Mo–Au) deposits related to melting of thickened mafic lower crust: examples from the eastern Tethyan metallogenic domain. Ore Geol. Rev. 39, 21–45.
Hou, Z.Q., Zheng, Y.C., Yang, Z.M., Rui, Z.Y., Zhao, Z.D., Jiang, S.H., Qu, X.M., Sun, Q.Z., 2013. Contribution of mantle components within juvenile lower-crust to collisional zone porphyry Cu systems in Tibet. Mineral. Deposita 48, 173–192.
Hu, R.Z., Burnard, P.G., Bi, X.W., Zhou, M.F., Pen, J.T., Su, W.C., Wu, K.X., 2004. Helium and argon isotope geochemistry of alkaline intrusion-associated gold and copper deposits along the Red River–Jingshajiang fault belt, SW China. Chem. Geol. 203, 305–317.
Jiang, Y.H., Jiang, S.Y., Ling, H.F., Dai, B.Z., 2006. Low-degree melting of a metasomatized lithospheric mantle for the origin of Cenozoic Yulong monzogranite-porphyry, east Tibet: geochemical and Sr–Nd–Pb–Hf isotopic constraints. Earth Planet. Sci. Lett. 241, 617–633.
Kapp, P., Yin, A., Harrison, T.M., Ding, L., 2005. Cretaceous-Tertiary shortening, basin development, and volcanism in central Tibet. Geol. Soc. Am. Bull. 117, 865–878.
Lan, T.G., Hu, R.Z., Bi, X.W., Mao, G.J., Wen, B.J., Liu, L., Chen, Y.H., 2017. Metasomatized asthenospheric mantle contributing to the generation of Cu- Mo deposits within an intracontinental setting: a case study of the 128 Ma Wangjiazhuang Cu-Mo deposit, eastern North China Craton. J. Asian Earth Sci. 160, 460–489. https://doi.org/10.1016/j.jseaes.2017.07.014.
Landtwing, M.R., Pettke, T., Halter, W.E., Heinrich, C.A., Redmond, P.B., Einaudi, M.T., Kunze, K., 2005. Copper deposition during quartz dissolution by cooling magmatic–hydrothermal fluids: the Bingham porphyry. Earth Planet. Sci. Lett. 235, 229–243.
Li, Y.Q., Rui, Z.Y., Cheng, L.X., 1981. Fluid inclusions and mineralization of the Yulong porphyry copper (Mo) deposit. Acta Geol. Sin. 55, 18–23 (in Chinese with English abstract).
Li, Y.S., L, Z,.C., Yan, G.S., Zhen, S.M., Du, Z,.Z., 2012a. Isotopic characteristics of S, Pb, H and O of Jiama copper-polymetallic ore deposit, Tibet, and their significance. Earth Sci. Front. 19, 72–81 (in Chinese with English abstract).
Li, J.X., Qin, K.Z., Li, G.M., Cao, M.J., Xiao, B., Chen, L., Zhao, J.X., Evans, N.J., McInnes, B.I.A., 2012b. Petrogenesis and thermal history of the Yulong porphyry copper deposit, Eastern Tibet: insights from U–Pb and U–Th/He dating, and zircon Hf isotope and trace element analysis. Mineral. Petrol. 105, 201–221.
Liang, H.Y., Campbell, I.H., Allen, C., Sun, W.D., Liu, C.Q., Yu, H.X., Xie, Y.W., Zhang, Y.Q., 2006. Zircon Ce^{4+}/Ce^{3+} ratios and ages for Yulong ore-bearing porphyries in eastern Tibet. Mineral Deposits 41, 152–159.
Liang, H.Y., Sun, W.D., Su, W.C., Zartman, R.E., 2009. Porphyry copper-gold mineralization at Yulong, China, promoted by decreasing redox potential during magnetite alteration. Econ. Geol. 104 (4), 587–596.
Lu, Y.F., 2004. GeoKit-A geochemical toolkit for Microsoft excel. Geochimica 33 (5), 459–464 (in Chinese with English abstract).
Meng, X.J., Hou, Z.Q., Li, Z.Q., 2006. Sulfur and lead isotope compositions of the Qulong porphyry copper deposit, Tibet: implications for the sources of plutons and metals in the deposit. Acta Geol. Sin. 80, 6–10 (in Chinese with English abstract).
Mukasa, S.B., Vidal, C.E., Injoque-Espinoza, J., 1990. Pb isotope bearing on the metallogenesis of sulfide ore deposits in central and southern Peru. Econ. Geol. 85, 1438–1446.
Ohmoto, H., 1972. Systematics of sulfur and carbon isotopes in hydrothermal ore deposits. Econ. Geol. 67, 551–578.
Ohmoto, H., Rye, R.O., 1979. Isotopes of sulphur and carbon. In: Barnes, H.L. (Ed.), Geochemistry of Hydrothermal Ore Deposits. Wiley, New York, pp. 509–−567.
Pettke, T., Oberli, F., Heinrich, C.A., 2010. The magma and metal source of giant porphyry-type ore deposits, based on lead isotope microanalysis of individual fluid inclusions. Earth Planet. Sci. Lett. 296, 267–277.
Qin, K.Z., Xia, D.X., Li, G.M., Xiao, B., Duo, J., Jiang, G.W., Zhao, J.X., 2014. Qulong Porphyry-Skarn Cu-Mo Deposit, Tibet. Science Press, Beijing (In Chinese).
Qu, X.M., Hou, Z.Q., Li, Y.G., 2002. Implications of S and Pb isotopic compositions of the Gangdese porphyry copper belt for the ore forming material source and material recycling within the orogenic belt. Geol. Bull. China 21 (11), 768–776 (in Chinese with English abstract).
Reich, M., Deditius, A., Chryssoulis, S., Li, J.W., Ma, C.Q., Parada, M.A., Barra, F., Mittermaya, F., 2013. Pyrite as a record of hydrothermal fluid evolution in a porphyry copper system: a SIMS/EMPA trace element study. Geochim. Cosmochim. Acta 104 (1), 42–62.
Richards, J.P., 2003. Tectono-magmatic precursors for porphyry Cu–(Mo–Au) deposit formation. Econ. Geol. 98, 1515–1533.
Richards, J.P., 2009. Post-subduction porphyry Cu–Au and epithermal Au deposits: products of remelting of subduction-modified lithosphere. Geology 37, 247–250.
Richards, J.P., 2011. Magmatic to hydrothermal metal fluxes in convergent and collided margins. Ore Geol. Rev. 40, 1–26.
Richards, J.P., 2015. Tectonic, magmatic, and metallogenic evolution of the Tethyan orogen: from subduction to collision. Ore Geol. Rev. 70, 323–345.
Richards, J.P., Mcculloch, M.T., Chappell, B.W., Kerrich, R., 1991. Sources of metals in the Porgera gold deposit, Papua New Guinea: evidence from alteration, isotope, and noble metal geochemistry. Geochim. Cosmochim. Acta 55 (2), 565–580.
Rye, R.O., 1993. The evolution of magmatic fluids in the epithermal environment: the stable isotope perspective. Econ. Geol. 88 (3), 733–752.
Sasaki, A., Ulriksen, C.E., Sato, K., Ishihara, S., 1984. Sulphur isotope reconnaissance of porphyry copper and manto-type deposits in Chile and the Philippines. Bull. Geol. Surv. Jpn. 35, 615–622.
Seal, R.R.I.I., 2006. Sulfur isotope geochemistry of sulfide minerals. Rev. Mineral. Geochem. 61, 633–677.
Shafiei, B., 2010. Lead isotope signatures of the igneous rocks and porphyry copper deposits from the Kerman Cenozoic magmatic arc (SE Iran), and their magmatic-metallogenetic implications. Ore Geol. Rev. 38 (1), 27–36.
Shafiei, B., Haschke, M., Shahabpour, J., 2009. Recycling of orogenic arc crust triggers porphyry Cu mineralization in Kerman Cenozoic arc rocks, southeastern Iran. Mineral. Deposita 44, 265–283.
Sillitoe, R.H., 1972. A plate tectonic model for the origin of porphyry copper deposits. Econ. Geol. 67, 184–197.
Sillitoe, R.H., 2010. Porphyry copper systems. Econ. Geol. 105, 3–41.
Steiger, R.H., Jäger, E., 1977. Subcommission on geochronology: convention on the use of decay constants in geo- and cosmochronology. Earth Planet. Sci. Lett. 36, 359–362.
Tang, R.L., Luo, H.S., 1995. The Geology of Yulong Porphyry Copper (Molybdenum) Ore Belt, Xizang (Tibet): Beijing. Geological Publishing House (320 p (in Chinese with English abstract)).
Tang, J.X., Wang, C.H., Qu, W.J., Du, A.D., Ying, L.J., Gao, Y.M., 2009. Re-Os isotopic dating of molybdenite from the Yulong porphyry Copper-Molybdenum deposit in Tibet and its metallogenic significance. Rock Miner. Anal. 28 (3), 215–218 (in Chinese with English abstract).
Tibet Yulong Copper Co., Ltd., 2009. Yulong Copper Polymetallic Deposit Exploration Report. Jomda County, Tibet.
Todt, W., Cliff, R.A., Hanser, A.W., Hofmann, A.W., 1993. Re-calibration of NBS lead standards using a $^{202}Pb+^{205}Pb$ double spike. Terra Abstracts 5, 396.
Todt, W., Cliff, R.A., Hanser, A.W., 1996. Evolution of a Pb–Pb double spike for high precision lead isotope analysis. In: Basu, A., Hart, S. (Eds.), Earth Processes: Reading the Isotope Code. Geophysical Monograph 95, pp. 429–437.
Tosdal, R.M., Munizaga, F., 2003. Lead sources in Mesozoic and Cenozoic Andean ore deposits, north-central Chile (30–34S). Mineral. Deposita 38, 234–250.
Tosdal, R.M., Wooden, J.L., Bouse, R.M., 1999. Pb isotopes, ore deposits, and metallogenic terranes. Soc. Econ. Geol. Rev. Econ. Geol. 12, 1–12.
Wang, J.H., Yin, A., Harrison, T.M., Grove, M., Zhang, Y.Q., Xie, G.H., 2001. A tectonic model for Cenozoic igneous activities in the eastern Indo–Asian collision zone. Earth Planet. Sci. Lett. 188 (1), 123–133.
Wang, D., Bi, X.W., Lu, H.Z., Hu, R.Z., Wang, X.S., Xu, L.L., 2018. Fluid and melt inclusion study on mineralized and barren porphyries, Jinshajiang-Red river alkali-rich intrusive belt, and significance to metallogenesis. J. Geochem. Explor. 184, 28–39.
Wilson, A.J., Cooke, D.R., Harper, B.J., Deyell, C.L., 2007. Sulfur isotopic zonation in the Cadia district, southeastern Australia – Exploration significance and implication for the genesis of alkalic porphyry gold–copper deposits. Mineral. Deposita 42, 465–487.
Xu, L.L., Bi, X.W., Su,W.C., Qi, Y.Q., Li, L., Chen, Y.W., Dong, S.H., Tang, Y.Y., 2011. Geochemical characteristics and petrogenesis of the quartz syenite porphyry from Tongchang porphyry Cu(Mo–Au) deposit in Jinping County, Yunan Province. Acta Petrol. Sin. 27, 3109–3122 (in Chinese with English abstract).
Xu, L.L., Bi, X.W., Hu, R.Z., Zhang, X.C., Su, W.C., Qu, W.J., Hu, Z.C., Tang, Y.Y., 2012. Relationships between porphyry Cu–Mo mineralization in the Jinshajiang–Red River metallogenic belt and tectonic activity: constraints from zircon U–Pb and molybdenite Re–Os geochronology. Ore Geol. Rev. 48, 460–473.
Xu, L.L., Bi, X.W., Hu, R.Z., Tang, Y.Y., Wang, X.S., Xu, Y., 2015. LA–ICP–MS mineral chemistry of titanite and the geological implications for exploration of porphyry Cu deposits in the Jinshajiang–Red River alkaline igneous belt, SW China. Mineral. Petrol. 109 (2), 181–200.
Xu, L.L., Bi, X.W., Hu, R.Z., Qi, Y.Q., Tang, Y.Y., Wang, X.S., Zhu, J.J., 2016. Redox states and genesis of magmas associated with intra-continental porphyry Cu–Au mineralization within the Jinshajiang–Red river alkaline igneous belt, SW China. Ore Geol. Rev. 73, 330–345.
Yang, X.M., 2012. Sulphur solubility in felsic magmas: implications for genesis of intrusion-related gold mineralization. Geosci. Can. 39, 17–32.
Yin, A., Harrison, T.M., 2000. Geologic evolution of the Himalayan–Tibetan orogen. Annu. Rev. Earth Planet. Sci. 28, 211–280.
Zartman, R.E., Doe, B.R., 1981. Plumbotectonics – the model. Tectonophysics 75, 135–162.
Zhang, Y.Q., Xie, Y.W., Qiu, H.N., Li, X.H., Zhong, S.L., 1998a. Shoshonitic series: Geochemical characteristics of elements for ore-bearing porphyry from Yulong copper ore belt in eastern Tibet. Earth Sci. J. China Univ. Geosci. 23, 557–561 (in Chinese).
Zhang, Y.Q., Xie, Y.W., Qiu, H.N., Li, X.H., Zhong, S.L., 1998b. Shoshonitic series: Sr, Nd, and Pb isotopic compositions of ore-bearing porphyry for Yulong copper ore belt in Eastern Tibet. Sci. Geol. Sin. 33, 359–366 (in Chinese with English abstract).
Zhang, J.C., Lin, Y.T., Yang, W., Shen, W.J., Hao, J.L., Hu, S., Cao, M.J., 2014. Improved precision and spatial resolution of sulfur isotope analysis using Nano-SIMS. J. Anal. At. Spectrom. 29, 1934–1943.
Zhang, Y.Q., Xie, Y.W., 1997. The geochronology and Nd, Sr isotopic characteristics of the Ailaoshan-Jinshajiang alkali-rich intrusive belt. Sci. China Ser. D Earth Sci. 4,

289–293 (in Chinese).
Zheng, S.J., 2017. The Research on Mineralogy and Geochemistry from Jiama Porphyry-skarn Copper-polymetallic System (Master thesis). Institute of Geochemistry, Chinese Academy of Sciences, Guiyang (in Chinese).
Zheng, Y.F., Chen, J.F., 2000. Stable Isotope Geochemistry. Science Press, Beijing, pp. 1–336 (in Chinese).
Zhou, Q., Jiang, Y.H., Zhang, H.H., Liao, S.Y., Jin, G.D., Zhao, P., Jia, R.Y., Liu, Z., 2012. Mantle origin of the Dexing porphyry copper deposit, SE China. Int. Geol. Rev. 55 (3), 337–349.
Zhu, J.J., Hu, R.Z., Bi, X.W., Zhong, H., Chen, H., 2011. Zircon U-Pb ages, Hf-O isotopes and whole-rock Sr-Nd-Pb isotopic geochemistry of granitoids in the Jinshajiang suture zone, SW China: Constraints on petrogenesis and tectonic evolution of the Paleo-Tethys Ocean. Lithos 126, 248–264.
Zi, J.W., Cawood, P.A., Fan, W.M., Tohver, E., Wang, Y.J., McCuaig, T.C., 2012a. Generation of Early Indosinian enriched mantle-derived granitoid pluton in the Sanjiang Orogen (SW China) in response to closure of the Paleo-Tethys. Lithos 140–141, 166–182.
Zi, J.W., Cawood, P.A., Fan, W.M., Wang, Y.J., Tohver, E., McCuaig, T.C., Peng, T.P., 2012b. Triassic collision in the Paleo-Tethys Ocean constrained by volcanic activity in SW China. Lithos 144–145, 145–160.